

1 **An observation-constrained multi-physics WRF ensemble for simulating European**
2 **mega heat waves**

3 Annemiek I. Stegehuis¹, Robert Vautard¹, Philippe Ciais¹, Adriaan J. Teuling², Diego G.
4 Miralles^{3,4} and Martin Wild⁵

5

6 ¹ LSCE/IPSL, Laboratoire CEA/CNRS/UVSQ, Gif-sur-Yvette, France

7 ² Hydrology and Quantitative Water Management Group, Wageningen University, The
8 Netherlands

9 ³ Department of Earth Sciences, VU University Amsterdam, Amsterdam, The Netherlands

10 ⁴ Laboratory of Hydrology and Water Management, Ghent University, Ghent, Belgium

11 ⁵ ETH Zurich, Zurich, Switzerland

12

13

14 Corresponding author : A.I. Stegehuis, LSCE/IPSL, Laboratoire CEA/CNRS/UVSQ, 91191

15 Gif-sur-Yvette CEDEX, France

16

17 **Abstract**

18 Climate models are not often evaluated or calibrated against observations of past climate
19 extremes, resulting in poor performance during for instance heat wave conditions. Here we
20 use the [Weather Research and Forecasting](#) (WRF) regional climate model with a large
21 combination of different atmospheric physics schemes, with the goal of detecting the most
22 sensitive physics and identifying those that appear most suitable for simulating the heat wave
23 events of 2003 in Western Europe and 2010 in Russia. 55 out of 216 simulations combining
24 different atmospheric physical schemes have a temperature bias smaller than 1 degree during
25 the heat wave episodes, the majority of simulations showing a cold bias of on average 2-3°C.
26 Conversely, precipitation is mostly overestimated prior to heat waves, and short wave
27 radiation is slightly overestimated. Convection is found to be the most sensitive atmospheric
28 physical process impacting simulated heat wave temperature, across four different convection
29 schemes in the simulation ensemble. Based on these comparisons, we design a reduced
30 ensemble of five well performing and diverse scheme combinations, which may be used in the
31 future to perform heat wave analysis and to investigate the impact of climate change in
32 summer in Europe. Future studies could include the sensitivity to land surface processes
33 controlling soil moisture, through the use of varied land surface models together with varied
34 physics schemes.

35 **1. Introduction**

36 An increasing number of simulations and studies project a higher frequency of several types
37 of extreme weather events in the future (e.g. Schär et al., 2004; Meehl et al., 2004; Della-
38 Marta et al., 2007; Beniston et al., 2007; Kuglitsch et al., 2010; Fischer and Schär, 2010;
39 Seneviratne et al., 2012; Orłowsky and Seneviratne, 2012). Since summer heat waves are
40 among the most problematic of such phenomena - threatening society and ecosystems -

41 climate models used for future projections must provide accurate simulations of these
42 phenomena, or at least their uncertainties should be documented. Even if climate models have
43 been evaluated using observed weather in past decades, it is unclear whether they will be able
44 to simulate extreme heat waves in future climates that may not have analogues in the
45 historical record. At least, models should be able to reproduce the conditions measured during
46 recent extreme heat wave cases, some of them having been shown to be unprecedented when
47 considering the climate over the past five or six centuries (Chuine et al., 2004; Luterbacher et
48 al., 2010; García-Herrera et al., 2010; Barriopedro et al., 2011; Tingley and Huybers, 2013).

49 Given the importance of forecasting summer heat waves well in advance, many studies have
50 analyzed their predictability, which remains poor in seasonal forecasts. For instance the 2003
51 European heat wave was not simulated realistically (neither timing nor intensity) by the
52 operational European Centre for Medium-Range Weather Forecasts (ECMWF) system, but
53 improvements were clear with the use of a new soil, convection and radiation schemes (e.g.
54 Weisheimer et al., 2011; Dole et al. 2011; Koster et al. 2010; van den Hurk et al. 2012).
55 However seasonal forecasting experiments do not easily allow the assessment of model
56 physical processes underlying extreme temperatures during heat waves because model biases
57 are mixed with sensitivity to initial conditions. These may inhibit the effect of the
58 representation of physical processes in reproducing the exact atmospheric circulation when
59 starting simulations at the beginning of the season.

60 From a statistical perspective, extreme temperatures have been found to be reasonably well
61 represented in global simulations of the current climate (IPCC, 2013), as well as in regional
62 simulations (Nikulin et al., 2010). In recent regional modeling evaluation experiments, using
63 an ensemble of state-of-the-art regional models guided by re-analysis at the boundaries of a
64 European domain, summer extreme seasonal temperatures were shown to be simulated with
65 biases in the range of a few degrees (Vautard et al., 2013). Individual mega heat waves (2003

66 in Western Europe, 2010 in Russia) were reproduced by most models. However, it was
67 difficult to infer whether these models could also simulate associated processes leading to the
68 extreme heat waves. The exact same events with similar atmospheric flow and its persistence
69 could not be reproduced due to internal variability of the models.

70 A comprehensive assessment of simulations of recent mega heat waves has only been the
71 object of a limited number of such studies. Process-oriented studies of high extreme
72 temperatures over Europe have focused on land-atmosphere feedbacks (e.g. Seneviratne et al.,
73 2006 and 2010; Fischer et al., 2007; Teuling et al., 2009; Stegehuis et al., 2013; Miralles et al.,
74 2014) because, beyond atmospheric synoptic circulation, these feedbacks are known to play
75 an important role in summer heat waves. However, the sensitivity of simulated heat wave
76 conditions to physical processes in models has not yet been explored in a systematic way.
77 This could be important because error compensation among processes that involve land-
78 atmosphere interactions, radiation and clouds may cause high temperatures for the wrong
79 reasons (Lenderink et al., 2007).

80 The goal of the present study is threefold. First we examine the ability of a regional climate
81 model, the Weather Research and Forecast (WRF, Skamarock et al., 2008), to simulate recent
82 European mega heat waves, with a number of different model configurations. Analysis of
83 these experiments then allows understanding which physical parameterizations are prone to
84 reproduce the build-up of extreme temperatures, and thus the need for carefully constraining
85 them in order to simulate these events properly. Finally, using observational constraints of
86 temperature, precipitation and radiation, we select a reduced ensemble of WRF configurations
87 that best simulates European heat waves, with different sets of physical schemes combinations.
88 This constrained multi-physics ensemble aims therefore at spanning a range of possible
89 physical parameterizations in extreme heat wave cases while keeping simulations close to
90 observations.

91 Our multi-physics regional ensemble approach contrasts with the classical multi-model
92 ensembles that are constructed by the availability of model simulations in coordinated
93 experiments (see e.g. Déqué et al., 2007 and references therein) or combinations of
94 parameterizations selected by different groups using the same model system (García-Díez et
95 al., 2014). In the latter “democracy-driven” ensemble, the lack of overall design strategy may
96 lead the uncertainty estimation to be biased and the models to be farther from observations. In
97 addition, the real cause of model spread is difficult to understand because of interacting
98 physical processes and their biases. Regional perturbed-physics or multi-physics ensembles
99 could help understand and constrain uncertainties more effectively, but so far they have been
100 seldom explored. García-Díez et al. (2014) showed that even a small multi-physics ensemble
101 confronted to several climate variable observations can help diagnose mean biases of a RCM.
102 Bellprat et al. (2012) showed that a well-constrained perturbed physics ensemble may
103 encompass the observations. Their perturbed physics ensemble was designed by varying the
104 values of a number of free parameters, and selecting only the configurations that were closest
105 to the observations; however, the number of combinations of different physical
106 parameterization schemes was limited to a total of eight different configurations.

107 The WRF model offers several parameterization schemes for most physical processes, and is
108 thus suitable for a multi-physics approach. In fact, a WRF multi-physics approach has been
109 used in several studies (e.g. García-Díez et al., 2011; Evans et al., 2012; Awan et al., 2011;
110 Mooney et al., 2013), also with its predecessor MM5, but not specifically to simulate extreme
111 heat waves.

112 Here we run an ensemble of 216 combinations of WRF physical parameterizations, and
113 compare each simulation with a set of observations of relevant variables in order to select a
114 reduced set of 5 combinations that best represent European summer mega heat waves. The
115 evaluation is made over the extreme 2003 and 2010 events. The ensemble is also evaluated

116 for a more regular summer (2007) in order to test the model configurations under non-heat
117 wave conditions.

118 **2. Methods**

119

120 *Simulations and general model setup*

121 We use the WRF version 3.3.1 and simulate the three summers (2003, 2007, 2010) using an
122 ensemble of physics scheme combinations. We first test the time necessary to initialize the
123 soil moisture on a limited number of cases. Soil conditions are initialized using the ERA-
124 Interim (Dee et al., 2011) soil moisture and temperatures; thereafter soil moisture and air
125 temperature are calculated as prognostic variables by WRF. For the August 2003 case, we
126 find that temperatures differ by less than 0.5°C among one another when starting experiments
127 before May 1st. Thus in the current study, each simulation is run from the beginning of May to
128 the end of August for the years 2003, 2007 and 2010. The regional domain considered is the
129 EURO-CORDEX domain (Jacob et al., 2014; Vautard et al., 2013) and the low-resolution
130 setup of 50 km x 50 km (~0.44 degree on a rotated lat-lon grid) is used – note that Vautard et
131 al. (2013) recently concluded that a higher spatial resolution did not provide a substantial
132 improvement in heat wave simulations. We use a vertical resolution with 32 levels for WRF.
133 Boundary conditions come from ERA-Interim (as well as initial snow cover, soil moisture and
134 temperature). In order to focus on physical processes in the boundary layer and the soil-
135 atmosphere interface, and to avoid chaotic evolution of large-scale atmospheric circulation,
136 we constrain the model wind fields with ERA-Interim re-analyses above Model Level #15
137 (about 3000m), similar to previous studies (Vautard et al., 2014), using grid nudging, with a
138 relaxation coefficient of $5 \cdot 10^{-5} \text{ s}^{-1}$, corresponding to a relaxation time about equivalent to the
139 input frequency (every six hours) (Omrani et al., 2013). Temperature and water vapor were
140 not constrained, to let feedbacks fully develop.

141 *Physics schemes*

142 We test 216 combinations of physics schemes. We consider different physics of the planetary
143 boundary layer and surface layer (PBL; 6 schemes), microphysics (MP; 3 schemes), radiation
144 (RA; 3 schemes) and of convection (CU; 4 schemes). For each type of scheme, a few options
145 were selected among the ensemble of possibilities offered in WRF. The selection was made to
146 avoid variants of the same scheme, and to maximize the difference of temperature and
147 precipitation outputs in preliminary experiments. At the time of study and model development
148 stage, different land-surface schemes were available in WRF: 5-layer Thermal Diffusion
149 Scheme (Dudhia, 1996), NOAH (Tewari et al., 2004), Rapid Update Cycle (RUC) (Benjamin
150 et al., 2004) and Pleim-Xiu (Gilliam & Pleim, 2010). We decided however to only use one,
151 the NOAH land surface scheme, in order to focus our study on atmospheric processes while
152 limiting the number of simulations, and because the NOAH scheme is the most widely used in
153 WRF applications. This was also motivated by the poor performance and extreme sensitivity
154 of the RUC land surface scheme for the land latent and sensible heat flux as compared with
155 local observations in 2003. It simulates strong latent heat fluxes in the beginning of the season
156 and an extreme drying at the end, while sensible heat flux is overestimated. The NOAH
157 scheme seemed more stable in the tests that were done for capturing both latent and sensible
158 heat fluxes during the 2003 heat wave at selected flux tower sites in Western Europe (Figure
159 1). Furthermore the Pleim-Xiu scheme is especially recommended for retrospective air quality
160 simulations, and is developed with a specific surface layer scheme as coupled configuration
161 (Gilliam & Pleim, 2010). The last possible option is the 5-layer thermal diffusion scheme
162 (Dudhia, 1996) which predicts ground and soil temperatures but no soil moisture, and is
163 therefore also not suitable for our study. Table 1 describes the physical schemes that were
164 combined to simulate the weather over the three summer seasons.

165 *Observational data*

166 In order to evaluate the ensemble and to rank and select its best performing simulations we
167 use gridded observed daily temperature and precipitation from E-OBS with a 0.25 degree
168 resolution (version 7.0) (Haylock et al., 2008). Bilinear interpolation is used to regrid E-OBS
169 data and the model output to the same grid. Furthermore we use station data of monthly global
170 radiation from the Global Energy Balance Archive (GEBA) network (Wild et al., 2009). For
171 France 2003 the data of 21 stations were available, for 2007 this number was 20. Observations
172 over Russia were too scarce, and were not considered. Model data are interpolated to these
173 stations using the nearest neighbor method. In addition, in order to check land-atmosphere
174 fluxes and the partitioning of net radiation into sensible and latent heat fluxes, we use the
175 satellite observation-driven estimates of daily latent heat fluxes from GLEAM (Miralles et al.,
176 2011). Since the latter is not a direct measurement we do not use them to validate and rank the
177 model configurations. Furthermore latent- and sensible heat flux measurements are used from
178 three FLUXNET sites from the Carbo-Extreme database (Neustift/Stubai – Austria
179 (Wohlfahrt et al., 2010); Tharandt-Anchor station – Germany (Grünwald & Bernhofer,
180 2007); and Soroe-LilleBogeskov – Denmark (Pilegaard et al., 2009)), for the evaluation of the
181 land surface schemes.

182 *Evaluation and ranking of model simulations*

183 For ranking, we set up several measures of model skill, based on the differences between
184 observed and simulated spatial averages over two domains: France for 2003 and 2007 (5W–
185 5E & 44N–50N), and one in Russia for 2007 and 2010 (25E–60E & 50N–60N) (Fig. 2). A
186 first scheme selection is made based on the skill to reproduce air temperature dynamics, since
187 this is the primary impacted variable and observations are reliable. Because we are interested
188 in heat waves, we select only those simulations that are within a 1 K regional average
189 difference between simulated and observed temperature, for heat wave periods; these periods
190 are defined as August 1st-15th for France (in 2003), and July 1st till August 15th for Russia (in

2010). The 1 K threshold is arbitrary but is used to avoid processing a large number of simulations that have unrealistic temperatures. Only 55 of the 216 simulations meet this criterion and are further considered. Then, the ranking of the retained simulations is done based on: (i) the daily temperature difference between simulations and observations during the heat wave periods (as above for 2003 and 2010), and during the period 1st-31st August for the normal year 2007, (ii) the root mean square error of monthly precipitation and radiation for the months July, June and August. The GEBA data set only contains scarce radiation observations over Russia, and therefore we could not consider this region for ranking models against incoming shortwave radiation. As a final step, an overall ranking is proposed by averaging the ranks obtained from the three variables (temperature, precipitation and radiation). From this final ranking, and in order to select an elite of multi-physics combinations, we selected the top-5 highest-ranked configurations. Note that observational uncertainty is not considered in this study, which is shown to be able to impact model ranking over Spain (Gomez-Navarro et al., 2012).

3. Results

3.1. Large systematic errors found during heat wave periods

Figure 3 shows the large temperature range spanned by the 216 ensemble members for the spatial average over the heat wave areas. The min-max range between ensemble members is up to 5°C during heat wave periods (Figure 3). Locally at 50 km resolution, the difference between the warmest and the coldest simulation during a heat wave is larger, reaching more than 10°C in 2003 (Figure 3d). In 2007, when summer temperatures were not extreme, the range is about twice as small. Only a few simulations match the observed high temperatures (Figure 3a-c). In Fig. 3a, we select two extreme configurations (blue and red lines), based on daily mean temperature over France during the 2003 heat wave. Interestingly, they are

215 extreme in all regions and years, indicating that each combination tends to induce a rather
216 large systematic bias. This bias however, is different for the ‘warm’ and the ‘cold’
217 configuration. It seems not to be due to a misrepresentation of the diurnal cycle, since they
218 remain when analyzing time series of maximum and minimum daily temperatures
219 independently (see supplementary Figures 1a-f). However, minimum temperatures show a
220 less consistent bias than maximum daily temperatures. A systematic temperature
221 underestimation by WRF simulations over Europe has also been found in other multi-physics
222 ensemble studies over Europe (e.g. Awan et al., 2011; García-Díez et al., 2011, 2014).

223 For monthly precipitation we obtain a large range of simulated values, with most
224 configurations overestimating monthly summer rainfall (JJA) during heat waves years, and to
225 a lesser extent during the wetter 2007 season (Fig. 4a-c). This is in line with the findings
226 reported by Warrach-Sagi et al. (2013) and Awan et al. (2011), and with the overestimation of
227 precipitation by many EURO-CORDEX models shown by Kotlarski et al. (2014). The two
228 selected extreme combinations (based on temperature, as explained above) are reproducing
229 precipitation overall without a major bias. This suggests that the temperature bias in these two
230 extreme simulations is not explicitly caused by a misrepresentation of the atmospheric water
231 supply from precipitation. However soil moisture (the soil moisture over the whole column)
232 does show a strong relation to temperature biases in model simulations. Figure 5a-d shows
233 soil moisture at the end of July versus temperature in August 2003 for each model
234 configuration. Configurations with low soil moisture level are associated with higher
235 temperatures and vice versa, confirming the role of land-atmosphere feedbacks during heat
236 waves, already pointed out by previous studies. This indicates that the evapotranspiration
237 from spring to summer depleting soil moisture can be a critical process during summer for the
238 development of heat waves, and that this process is not simply related to summer
239 precipitation.

240 For solar radiation, the mean differences between our simulations over France 2003 and 2007
241 reaches approximately 100 Wm^{-2} (Fig. 6a,b). Observations for France (black dots) are found
242 below the median value of the simulations so a slight overestimation of the ensemble is
243 obtained. The first (warmest) extreme configuration (red dot) is associated with an
244 overestimated radiation of $10\text{-}50 \text{ Wm}^{-2}$ while the other (coldest, blue dot) extreme
245 configuration exhibits an underestimated radiation by about the same amount. Since the
246 warmest simulation agrees better with temperature observations than the coldest simulation,
247 one may therefore suspect that it contains a cooling mechanism that partly compensates for
248 the overestimated solar radiation.

249 **3.2. Sensitivity of temperatures to physical parameterizations and sources of spread**

250 In order to identify the physics schemes to which the development of heat waves is most
251 sensitive, we examine how resulting temperatures are clustered as a function of the scheme
252 used. We find that the spread between all simulations – both in terms of temperature and soil
253 moisture – is mostly due to the differences in convection scheme (clustering of dots with the
254 same color in Fig. 5a). For instance the Tiedtke scheme (blue dots) systematically leads to
255 higher temperatures and lower soil moisture, while the Kain-Fritsch scheme (green dots) leads
256 to wetter soils and lower temperatures, inhibiting heat waves. Microphysics and radiation
257 schemes are also contributing to the spread of simulated temperature and soil moisture values
258 (Fig. 5b-c), although their effect is less marked than for convection. Heat wave temperatures
259 and soil moisture seem to be least sensitive to the planetary boundary layer and surface layer
260 physics schemes. The sensitivity of the convection scheme in WRF has already been
261 mentioned in previous studies (Jankov et al., 2005; Awan et al., 2011;; Vautard et al., 2013;
262 García-Díez et al., 2014). Note that the soil moisture simulated in early August 2003 is better
263 correlated with preceding radiation than with precipitation (compare Supplementary Figures 2
264 and 3), indicating that the way clouds, and particularly convective clouds, affect radiation

265 prior to the onset of heat waves is a major driver of the spread for the development of heat
266 waves, higher radiation leading to drier soils and higher temperatures during heat waves.

267 **3.3. A constrained reduced ensemble of best simulations**

268 Focusing only on the 55 selected simulations that differ less than 1°C from the observations
269 during the heat waves, we apply the ranking method introduced in Section 2 based on
270 temperature, precipitation and radiation model-observation comparison metrics. The 5 highest
271 ranked simulations are given in Table 2 and are actually the numbers 1-5 in Supplementary
272 Table 1. Figure 7a confirms the ranking by showing that these simulations also perform well
273 in terms of temperature, during the months prior to the heat wave. The same is furthermore
274 found for the years 2007 in France (Supp. Fig. 5) and 2010 in Russia (Supp. Fig. 4), and also
275 for other regions such as the Iberian Peninsula and Scandinavia (Supp. Fig. 6a,d). The
276 selected simulations however performed less well for precipitation over France in 2003 (Fig.
277 7b), but do not show a large overestimation of precipitation either. Precipitation over Russia
278 for the 5 highest-ranked simulations does show good performance (Supp. Fig. 4b), as well as
279 for other European regions (Supp. Fig. 6). The mean radiation of the ensemble of the five best
280 simulations is closer to the GEBA observations than in the case of the original ensemble (Fig.
281 7c).

282 Nonetheless, the better match of the reduced ensemble of the five highest-ranked simulations
283 to the observations of temperature, precipitation and radiation is to a very large degree
284 unsurprising: the selection was based on the fit to observations. However, it is still
285 satisfactory to see that some simulations are capable of matching all three variables.
286 Conversely, we also compare simulations against another key variable that was not used for
287 evaluating and ranking simulations, namely the latent heat flux (Figure 7d). Albeit somehow
288 reduced compared to the full-ensemble spread, the spread of the five best simulations for the

289 latent heat flux remains large over the whole period, on average between 50 and 120 Wm^{-2}
290 (observed values are around 75 Wm^{-2}). However, during the 2003 heat wave over France
291 three of the five best simulations exhibit a close resemblance to the latent heat observations
292 (approximately 5-10 Wm^{-2}) (Fig. 7d). The two simulations that are found to considerable
293 overestimate latent heat flux by approximately 30-40 Wm^{-2} (as compared to GLEAM) are
294 those that use a different convection scheme than the Tiedtke scheme. The overestimation of
295 latent heat fluxes in these schemes is however not generalized for other regions and years
296 (Suppl. Fig. 4c, 5d, 6c,f-h), for which the latent heat flux was fairly well simulated within the
297 range of uncertainty of GLEAM.

298 A cross-comparison for the years 2003 and 2010, that is, using only the 2010 heat wave to
299 select schemes and verify the performance of the selected schemes over 2003 and vice versa,
300 yields some promising results. Table 3 shows the average ranking of the best (5, 10, 15, 20
301 and 25) simulations. When only using one heat wave to select the best configurations, they all
302 lie in the top-ranked half, and even higher in the ranking in the case of the 2010 heat wave
303 over Russia being used to select the best configurations. This suggests that the selection based
304 upon one heat wave in one region should also provide better simulations for other heat waves
305 or heat waves in other areas, i.e. that the bias of a member of the WRF ensemble is not local,
306 but at least regional at the scale of Western Europe.

307 **4. Concluding remarks**

308 In this study we designed and analyzed a large multi-physics ensemble with the WRF model.
309 It is made of all possible combinations of a set of different atmospheric physics
310 parameterization schemes. They were evaluated for their ability to simulate the European heat
311 waves of 2003 and 2010 using the regional climate model WRF based on temperature,
312 precipitation and shortwave radiation. Even though the simulations were constrained by grid

313 nudging, we found a large spread between the different physics for the simulations for
314 temperature, precipitation and incoming shortwave radiation, three variables we used to create
315 an overall configuration ranking. Most simulations systematically underestimate temperature
316 and overestimate precipitation during heat waves, a model pattern that was already found in
317 previous studies dealing with much smaller ensembles (e.g. Awan et al., 2011; García-Díez et
318 al., 2011; Warrach-Sagi et al., 2013). The spread among ensemble members is amplified
319 during the two extreme heat waves of study. Since we only considered a single land surface
320 scheme, it is probable that the ensemble spread would largely increase when incorporating the
321 uncertainty associated with modeling land surface processes. Nevertheless, considering only
322 atmospheric processes, the magnitude of the spread still reaches 5°C during the peak of the
323 heat waves.

324 We also showed that among atmospheric process parameterizations, the choice of a
325 convection scheme appears to dominate the ensemble spread. We found indications that the
326 large differences between convection schemes seem to occur mostly through radiation, and
327 therefore the way convective clouds affect the surface energy and water budget prior to and
328 during heat waves. Changes in incoming radiation cause changes in evapotranspiration and
329 therefore soil moisture, which may subsequently feed back on air temperature.

330 From this ensemble, we selected a small sub-ensemble with the five best combinations of
331 atmospheric physics schemes based on the fit to observations. These combinations capture
332 well the temperature dynamics during the mega heat waves of France and Russia, and they
333 perform better than other combinations in other regions of Europe. In addition, they are
334 consistent with independent latent heat flux data used for cross-validation. This indicates that
335 the constraints set for the selection reduce the uncertainty across the whole European
336 continent and points towards the creation of an optimized ensemble of WRF configurations
337 specific for heat waves, with reduced error compensations. A sub-ensemble that outperforms

338 a larger ensemble was also found by Herrera et al. (2010). The sub-ensemble based on mean
339 precipitation showed better results for extreme precipitation as well.

340 However a limitation of this study is the use of only one land-surface scheme; the five
341 selected WRF configurations may actually all be affected by systematic errors of the NOAH
342 land surface scheme. The importance of the selected land surface scheme is further confirmed
343 by the larger spread of the “best” ensemble for latent heat (in Wm^{-2}) than for shortwave
344 radiation. In order to mimic radically different land surface processes, a sensitivity test where
345 initial soil moisture was artificially increased and decreased by 20% all along the soil column
346 was conducted. Results confirm the sensitivity of the temperature simulations to soil moisture,
347 a variable partly controlled by the land surface scheme (Figure 8). The full answer to this
348 question is left for a future study in which different atmospheric schemes and surface schemes
349 will be jointly permuted.

350 Although our ensemble is trained on only summer conditions, our results have several
351 implications for climate modeling. First, the constrained WRF ensemble may be used in
352 future studies of climate change; each of the five members may exhibit a different sensitivity
353 to future climate change conditions, leading to a constrained exploration of the uncertainty.
354 Then it is important to notice that our study pinpoints the need to carefully design or adjust
355 the convection scheme for a proper representation of the summer climate during heat waves.
356 This is particularly important in order to evaluate the impacts of climate change on
357 ecosystems, health, carbon cycle, water and cooling capacity of thermal energy plants, since
358 heat waves in the mid latitudes are expected to be of the most impacting phenomena in a
359 human altered climate. Therefore, impact studies can be designed based on the selected
360 configurations.

361

362 **Acknowledgments**

363 AIS acknowledges CEA for funding as well as of the GHG-Europe FP7 project. AJT
364 acknowledges financial support from The Netherlands Organisation for Scientific Research
365 through Veni grant 016.111.002. P.C. acknowledges support of the ERC-SYG project P-
366 IMBALANCE. The authors acknowledge K. Pilegaard, A. Ibrom, C. Bernhofer, G. Wohlfahrt
367 and CarboEurope for sharing FLUXNET data.

368

369 **References**

- 370 Awan, N. K., H. Truhetz & A. Gobiet (2011) Parameterization-induced error characteristics
371 of MM5 and WRF operated in climate mode over the Alpine region: an ensemble-based
372 analysis. *Journal of Climate*, 24, 3107-3123, doi:10.1175/2011JCLI3674.1.
- 373 Barriopedro, D., E. M. Fischer, J. Luterbacher, R. Trigo & R. Garcia-Herrera (2011) The hot
374 summer of 2010: redrawing the temperature record map of Europe. *Science*, 332, 220-
375 224, doi: 10.1126/science.1201224.
- 376 Beljaars, A.C.M. (1994) The parameterization of surface fluxes in large-scale models under
377 free convection. *Quart. J. Roy. Meteor. Soc.*, 121, 255–270.
- 378 Bellprat, O., S. Kotlarski, D. Luthi & C. Schär (2012) Exploring perturbed physics ensembles
379 in a regional climate model. *Journal of Climate*, 25, 4582-4599, doi: 10.1175/JCLI-D-
380 11-00275.1.
- 381 Beniston, M., D. B. Stephenson, O. B. Christensen, C. A. T. Ferro, C. Frei, S. Goyette, K.
382 Halsnaes, T. Holt, K. Jylha, B. Koffi, J. Palutikof, R. Scholl, T. Semmler & K. Woth
383 (2007) Future extreme events in European climate: an exploration of regional climate
384 model projections. *Clim. Change*, 81, 71-95 , doi: 10.1007/s10584-006-9226-z.
- 385 Benjamin, S. G., G. A. Grell, J. M. Brown & T. G. Smirnova (2004) Mesoscale weather
386 prediction with RUC hybrid isentropic-terrain-following coordinate model. *Mon. Wea.*

387 *Rev*, 132, 473-494.

388 Chou, M.-D. & M. J. Suarez (1999) A solar radiation parameterization for atmospheric
389 studies. *NASA Tech. Memo 104606* 40, Greenbelt, Maryland.

390 Chuine, I., P. Yiou, N. Viovy, B. Seguin, V. Daux & E. L. Ladurie (2004) Historical
391 phenology: grape ripening as a past climate indicator. *Nature*, 432, 289-290, doi:
392 10.1038/432289a.

393 Collins, W. D., P. J. Rasch, B. A. Boville, J. J. Hack, J. R. McCaa, D. L. Williamson, J. T.
394 Kiehl, B. Brieglib, C. Bitz, S.-J. Lin, M. Zhang & Y. Dai (2004) Description of the
395 NCAR Community Atmosphere Model (CAM 3.0). NCAR Tech. Note NCAR/TN-
396 464+STR. 214 pp.

397 Dee, D. P., S. M. Uppala, A. J. Simmons, P. Berrisford, P. Poli, S. Kobayashi, U. Andrae, M.
398 A. Balmaseda, G. Balsamo, P. Bauer, P. Bechtold, A. C. M. Beljaars, L. van de Berg, J.
399 Bidlot, N. Bormann, C. Delsol, R. Dragani, M. Fuentes, A. J. Geer, L. Haimberger, S.
400 B. Healy, H. Hersbach, E. V. Hólm, L. Isaksen, P. Kållberg, M. Köhler, M. Matricardi,
401 A. P. McNally, B. M. Monge-Sanz, J. J. Morcrette, B. K. Park, C. Peubey, P. de
402 Rosnay, C. Tavolato, J. N. Thépaut & F. Vitart (2011) The ERA-Interim reanalysis:
403 Configuration and performance of the data assimilation system. *Q. J. R. Meteorol. Soc.*,
404 137, 553-597.

405 Della-Marta, P.M., M. R. Haylock, J. Luterbacher & H. Wanner (2007) Doubled length of
406 western European summer heat waves since 1880. *J. Geophys. Res.*, 112, D15103,
407 doi:10.1029/2007JD008510.

408 Déqué, M, D. P. Rowell, D. Luthi, F. Giorgi, J. H. Christensen, B. Rockel, D. Jacob, E.
409 Kjellstrom, M. de Castro & B. van den Hurk (2007) An intercomparison of regional
410 climate simulations for Europe: assessing uncertainties in model projections. *Climatic*
411 *Change*, 81, 53-70, doi:10.1007/s10584-006-9228-x.

412 Dole, R., M. Hoerling, J. Perlwitz, J. Eischeid, P. Pegion, T. Zhang, X.-W. Quan, T. Y. Xu &
413 D. Murray (2011) Was there a basis for anticipating the 2010 Russian heat wave?
414 *Geophys. Res. Lett.*, 38, L06702, doi:10.1029/2010GL046582.

415 Dudhia, J. (1996) A multi-layer soil temperature model for MM5. Sixth Annual PSU/NCAR
416 Mesoscale Model Users' Workshop. Boulder CO, July 1996, 49-50.

417 Evans, J. P., M. Ekstrom & F. Ji (2012) Evaluating the performance of a WRF physics
418 ensemble over South-East Australia. *Clim. Dyn.*, 39, 1241-1258, doi:10.1007/s00382-
419 011-1244-5.

420 Fischer, E. M., S. I. Seneviratne, D. Luthi & C. Schär (2007) Contribution of land-atmosphere
421 coupling to recent European summer heat waves. *Geophys. Res. Lett.*, 34, L06707,
422 doi:10.1029/2006GL029068.

423 Fischer, E. M. & C. Schär (2010) Consistent geographical patterns of changes in high-impact
424 European heat waves. *Nat. Geosci.*, 3, 398-403.

425 García-Díez, M., J. Fernández, L. Fita & C. Yague (2011) Seasonal dependence of WRF
426 model biases and sensitivity to PBL schemes over Europe. *Q. J. R. Meteorol. Soc.*, 139,
427 501-514, doi:10.1002/qj.1976.

428 García-Díez, M., J. Fernández & R. Vautard (2014) An RCM multi-physics ensemble over
429 Europe : Multi-variable evaluation to avoid error compensation. *Clim. Dyn.*, submitted.

430 García-herrera, R., J. Diaz, R. M. Trigo, J. Luterbacher & E. M. Fischer (2010) A review of
431 the European summer heat wave of 2003. *Critical Reviews in Environmental Science
432 and Technology*, 40, 267-306, doi: 10.1080/10643380802238137.

433 Gomez-Navarro, J. J., J. P. Montávez, S. Jerez, P. Jimenez-Guerrero & E. Zorita (2012) What
434 is the role of the observational dataset in the evaluation and scoring of climate models?
435 *Geophys. Res. Lett.* 39:L24701.

436 Grell, G. A. & D. Devenyi (2013) A generalized approach to parameterizing convection
437 combining ensemble and data assimilation techniques. *Geophys. Res. Lett.*, 29, 1693,
438 doi:10.1029/2002GL015311.

439 Grünwald, T. & C. Bernhofer (2007) A decade of carbon, water and energy flux
440 measurements of an old spruce forest at the Anchor Station Tharandt. *Tellus*, 59B, 387–
441 396.

442 Han, J., & H. Pan (2011) Revision of convection and vertical diffusion schemes in the NCEP
443 Global Forecast System. *Wea. Forecasting*, 26, 520–533.

444 Haylock, M. R., N. Hofstra, A. M. G. Klein Tank, E. J. Klok, P. D. Jones & M. New (2008) A
445 European daily high-resolution gridded data set of surface temperature and precipitation
446 for 1950-2006. *J. Geophys. Res.*, 113, D20119, doi: 10.1029/2008JD010201.

447 Herrera, S., L. Fita, J. Fernández & J. M. Gutierrez (2010) "Evaluation of the mean and
448 extreme precipitation regimes from the ENSEMBLES regional climate multimodel" *J.*
449 *Geophys. Res.* 115:D21117.

450 Hong, S.-Y., & J.-O. J. Lim (2006a) The WRF single-moment 6-class microphysics scheme
451 (WSM6). *J. Korean Meteor. Soc.*, 42, 129–151.

452 Hong, S.-Y., Y. Noh, J. Dudhia (2006b) A new vertical diffusion package with an explicit
453 treatment of entrainment processes. *Mon. Wea. Rev.*, 134, 2318–2341.

454 Iacono, M. J., J. S. Delamere, E. J. Mlawer, M. W. Shephard, S. A. Clough & W. D. Collins
455 (2008) Radiative forcing by long-lived greenhouse gases: Calculations with the AER
456 radiative transfer models. *J. Geophys. Res.*, 113, D13103, doi:10.1029/2008JD009944.

457 IPCC, 2013: Climate Change 2013: The Physical Science Basis. Contribution of Working
458 Group I to the Fifth Assessment Report of the Intergovernmental Panel on Climate
459 Change [Stocker, T.F., D. Qin, G.-K. Plattner, M. Tignor, S.K. Allen, J. Boschung, A.
460 Nauels, Y. Xia, V. Bex and P.M. Midgley (eds.)]. Cambridge University Press,

461 Cambridge, United Kingdom and New York, NY, USA, 1535 pp,
462 doi:10.1017/CBO9781107415324.

463 Jacob, D., J. Petersen, B. Eggert, A. Alias, O. B. Christensen, L. M. Bouwer, A. Braun, A.
464 Colette, M. Deque, G. Georgievski, E. Georgopoulou, A. Gobiet, L. Menut, G. Nikulin,
465 A. Haensler, N. Hempelmann, C. Jones, K. Keuler, S. Kovats, N. Kroner, S. Kotlarski,
466 A. Kriegsmann, E. Martin, E. Van Meijgaard, C. Moseley, S. Pfeifer, S. Preuschmann,
467 C. Radermacher, K. Radtke, D. Rechid, M. Rounsevell, P. Samuelsson, S. Somot, J. F.
468 Soussana, C. Teichmann, R. Valentini, R. Vautard, B. Weber & P. Yiou (2014) EURO-
469 CORDEX: new-high-resolution climate change projections for European impact
470 research. *Regional Environmental Change*, 14, 563-578.

471 Janjic, Z. I. (1994) The Step–Mountain Eta Coordinate Model: Further developments of the
472 convection, viscous sublayer, and turbulence closure schemes. *Mon. Wea. Rev.*, **122**,
473 927–945.

474 Janjic, Z. I., (2002) Nonsingular implementation of the Mellor-Yamada Level 2.5 Scheme in
475 the NCEP Meso model. *NCEP Office Note No. 437*, 61 pp., National Centers for
476 Environmental Prediction, College Park, MD.

477 Jankov, I., W. A. Gallus, M. Segal, B. Shaw & S. E. Koch (2005) The impact of different
478 WRF model physical parameterizations and their interactions on warm season WCS
479 rainfall. *Weather and Forecasting*, 20, 1048-1060, doi:10.1175/WAF888.1.

480 Kain, J. S. (2004) The Kain–Fritsch convective parameterization: An update. *J. Appl. Meteor.*,
481 43, 170–181.

482 Koster, R. D., S. P. P. Mahanama, T. J. Yamada, G. Balsamo, A. A. Berg, M. Boisserie, P. A.
483 Dirmeyer, F. J. Doblas-Reyes, G. Drewitt, C. T. Gordon, Z. Guo, J. H. Jeong, D. M.
484 Lawrence, W. S. Lee, Z. Li, L. Luo, S. Malyshev, W. J. Merryfield, S. I. Seneviratne, T.
485 Stanelle, B. J. J. M. Van den Hurk, F. Vitart & E. F. Wood (2010) Contribution of land

486 surface initialization to subseasonal forecast skill: First results from a multi-model
487 experiment. *Geophys. Res. Lett.*, 37, L02402, doi: 10.1029/2009GL041677.

488 Kotlarski, S., K. Keuler, O. B. Christensen, A. Colette, M. Déqué, A. Gobiet, K. Goergen, D.
489 Jacob, D. Lüthi, E. van Meijgaard, G. Nikulin, C. Schär, C. Teichmann, R. Vautard, K.
490 Warrach-Sagi & V. Wulfmeyer (2014) Regional climate modeling on European scales:
491 a joint standard evaluation of the EURO-CORDEX RCM ensemble. *Geosci. Model*
492 *Dev.*, 7, 1297-1333, doi:10.5194/gmd-7-1297-2014, 2014.

493 Kuglitsch, F. G., T. Toreti, E. Xoplaki, P. M. Della-marta, C. S. Zerefos, M. Turkes & J.
494 Luterbacher (2010) Heat wave changes in the eastern Mediterranean since 1960.
495 *Geophys. Res. Lett.*, 37, L04802, doi: 10.1029/2009GL041841.

496 Lenderink, G., A. van Ulden, B. van den Hurk, E. van Meijgaard, 2007, Summertime inter-
497 annual temperature variability in an ensemble of regional model simulations: analysis of
498 the surface energy budget. *Climatic Change*, 81:233–247

499 Luterbacher, J., S. J. Koenig, J. Franke, G. Van der Schrier, E. Zorita, A. Moberg, J. Jacobeit,
500 P. M. Della-marta, M. Kuttel, E. Xoplaki, D. Wheeler, T. Rutishauser, M. Stossel, H.
501 Wanner, R. Brazdil, P Dobrovolny, D. Camuffo, C. Bertolin, A. Van Engelen, F. J.
502 Gonzalez-Rouco, R. Wilson, C. Pfister, D. Limanowka, O. Nordli, L. Leijonhufvud, J.
503 Soderberg, R. Allan, M. Barriendos, R. Glaser, D. Riemann, Z. Hao & C. S. Zerefos
504 (2010) Circulation dynamics and its influence on European and Mediterranean January-
505 April climate over the past half millennium: results and insights from instrumental data,
506 documentary evidence and coupled climate models. *Climate change*, 101, 201-234, doi:
507 10.1007/s10584-009-9782-0.

508 Meehl, G.A. & C. Tebaldi (2003) More intense, more frequent, and longer lasting heat waves
509 in the 21st century. *Science*, 305, 994-997, doi:10.1126/science.1098704.

510 Miralles, D. G., T. R. H. Holmes, R. A. M. De Jeu, J. H. Gash, A. G. C. A Meesters & A. J.
511 Dolman (2011) Global land-surface evaporation estimated from satellite-based
512 observations. *Hydrol. Earth Syst. Sci.*, 15, 453-469, doi:10.5194/hess-15-453-2011.

513 Miralles, D. G., A. J. Teuling, C. C. van Heerwaarden & J. Vilà-Guerau de Arellano (2014)
514 Mega-heatwave temperatures due to combined soil desiccation and atmospheric heat
515 accumulation. *Nature Geosci.*, 7, 345-349, doi:10.1038/ngeo2141.

516 Mooney, P. A., F. J. Mulligan & R. Fealy (2013) "Evaluation of the Sensitivity of the
517 Weather Research and Forecasting Model to Parameterization Schemes for Regional
518 Climates of Europe over the Period 1990–95", *J. Clim.* 26:1002-1017.

519 Morrison, H., G. Thompson & V. Tatarskii (2009) Impact of Cloud Microphysics on the
520 Development of Trailing Stratiform Precipitation in a Simulated Squall Line:
521 Comparison of One- and Two-Moment Schemes. *Mon. Wea. Rev.*, **137**, 991–1007.

522 Nakanishi, M. & H. Niino (2006) An improved Mellor–Yamada level 3 model: its numerical
523 stability and application to a regional prediction of advecting fog. *Bound. Layer
524 Meteor.*, 119, 397–407.

525 Nakanishi, M. & H. Niino (2009) Development of an improved turbulence closure
526 model for the atmospheric boundary layer. *J. Meteor. Soc. Japan*, **87**, 895–912.

527 Nikulin, G., E. Kjellstrom, U. Hansson, G. Strandberg and A. Ullerstig (2010) Evaluation and
528 future projections of temperature, precipitation and wind extremes over Europe in an
529 ensemble of regional climate simulations. *Tellus A*, 63, 41-55.

530 Omrani, H., P. Dobrinski, P & T. Dubos (2013) Optimal nudging strategies in regional
531 climate modelling: investigation in a Big-Brother experiment over the European and
532 Mediterranean regions. *Climate Dynamics*, 41, 2451-2470.

533 Orłowsky, B. & S. I. Seneviratne (2012) Global changes in extreme events: regional and
534 seasonal dimension. *Climatic Change*, 110, 669-696, doi:10.1007/s10584-011-0122-9.

535 Pilegaard, K., A. Ibrom, M. S. Courtney, P. Hummerlshøj & N. O. Jensen (2011) Increasing
536 net CO₂ uptake by a Danish beech forest during the period from 1996 to 2009.
537 *Agricultural and Forest Meteorology*, 151, 934-946.

538 Pleim, J. E. (2007) A Combined Local and Nonlocal Closure Model for the Atmospheric
539 Boundary Layer. Part I: Model Description and Testing. *J. Appl. Meteor. Climatol.*, 46,
540 1383–1395.

541 Schär, C., P. L. Vidale, D. Luthi, C. Frei, C. Haberli, M. A. Liniger & C. Appenzeller (2004)
542 The role of increasing temperature variability in European summer heatwaves. *Nature*,
543 427, 332-336, doi:10.1038/nature02300.

544 Seneviratne, S. I., D. Luthi, M. Litschi & C. Schär (2006) Land-atmosphere coupling and
545 climate change in Europe. *Nature*, 443, 205-209, doi: 10.1038/nature05095.

546 Seneviratne, S. I., T. Corti, E. L. Davin, M. Hirschi, E. B. Jaeger, I. Lehner, B. Orlowsky &
547 A. J. Teuling (2010) Investigating soil moisture-climate interactions in a changing
548 climate: a review. *Earth Sci. Rev.*, 99, 125-161.

549 Seneviratne, S. I., N. Nicholls, D. Easterling, C. M. Goodess, S. Kanae, J. Kossin, Y. Luo, J.
550 Marengo, K. McInnes, M. Rahimi, M. Reichstein, A. Sorteberg, C. Vera, and X. Zhang,
551 2012: Changes in climate extremes and their impacts on the natural physical
552 environment. In: *Managing the Risks of Extreme Events and Disasters to Advance
553 Climate Change Adaptation* [Field, C. B., V. Barros, T. F. Stocker, D. Qin, D. J.
554 Dokken, K. L. Ebi, M. D. Mastrandrea, K. J. Mach, G.-K. Plattner, S. K. Allen, M.
555 Tignor, and P. M. Midgley (eds.)]. A Special Report of Working Groups I and II of the
556 Intergovernmental Panel on Climate Change (IPCC). Cambridge University Press,
557 Cambridge, UK, and New York, NY, USA, pp. 109-230.

558 Skamarock, W. C., J. B. Klemp, J. Dudhia, D. O. Gill, D. M. Barker, M. G. Duda, X.-Y.
559 Huang, W. Wang & J. G. Powers (2008) A description of the Advanced Research WRF

560 version 3. NCAR Tech. Note 1–125, <http://nldr.library.ucar.edu/collections/TECH->
561 NOTE-000-000-000-855.

562 Stegehuis, A., R. Vautard, P. Ciais, A. J. Teuling, M. Jung & P. Yiou (2013) Summer
563 temperatures in Europe and land heat fluxes in observation-based data and regional
564 climate model simulations. *Clim. Dyn.*, 41, 455–477, doi:10.1007/s00382-012-1559-x.

565 Sukoriansky, S., B. Galperin, & V. Perov (2005) Application of a new spectral model of
566 stratified turbulence to the atmospheric boundary layer over sea ice. *Bound.–Layer
567 Meteor.*, 117, 231–257.

568 Teuling, A. J., M. Hirschi, A. Ohmura, M. Wild, M. Reichstein, P. Ciais, N. Buchmann, C.
569 Ammann, L. Montagnani, A. D. Richardson, G. Wohlfahrt & S. I. Seneviratne (2009) A
570 regional perspective on trends in continental evaporation. *Geophys. Res. Lett.*, 36,
571 L02404, doi: 10.1029/2008GL036584.

572 Tewari, M., F. Chen, W. Wang, J. Dudhia, M. A. LeMone, K. Mitchell, M. Ek, G. Gayno, J.
573 Wegiel & R. H. Cuenca (2004) Implementation and verification of the unified NOAA
574 land surface model in the WRF model. *20th conference on weather analysis and
575 forecasting/16th conference on numerical weather prediction*, pp. 11–15. Seattle, WA,
576 American Meteorological Society.

577 Thompson, G., P. R. Field, R. M. Rasmussen & W. D. Hall (2008) Explicit Forecasts of
578 Winter Precipitation Using an Improved Bulk Microphysics Scheme. Part II:
579 Implementation of a New Snow Parameterization. *Mon. Wea. Rev.*, 136, 5095–5115.

580 Tiedtke, M., (1989) A comprehensive mass flux scheme for cumulus parameterization in
581 large–scale models. *Mon. Wea. Rev.*, 117, 1779–1800.

582 Tingley, M. P. & P. Huybers (2013) Recent temperature extremes at high northern latitudes
583 unprecedented in the past 600 years. *Nature*, 496, 201–205, doi: 10.1038/nature11969.

584 Van den Hurk, B., F. Doblas-Reyes, G. Balsamo, R. D. Koster, S. I. Seneviratne & H.

585 Camargo (2012) Soil moisture effects on seasonal temperature and precipitation forecast
586 scores in Europe. *Clim. Dyn.*, 38, 349-362, doi: 10.1007/s00382-010-0956-2.

587 Vautard, R., A. Gobiet, D. Jacob, M. Belda, A. Colette, M. Deque, J. Fernandez, M. García-
588 Díez, K. Goergen, I. Guttler, T. Halenka, T. Karacostas, E. Katragkou, K. Keuler, S.
589 Kotlarski, S. Mayer, E. Van Meijgaard, G. Nikulin, M. Patarcic, J. Scinocca, S.
590 Sobolowski, M. Suklitsch, C. Teichmann, K. Warrach-Sagi, V. Wulfmeyer & P. Yiou
591 (2013) The simulation of European heat waves from an ensemble of regional climate
592 models within the EURO-CORDEX project. *Clim. Dyn.*, 41, 2555-2575,
593 doi:10.1007/s00382-013-1714-z.

594 Vautard, R., F. Thias, I. Tobin, F.-M. Breon, J.-G. Devezeaux de Lavergne, A. Colette, P.
595 Yiou & P. M. Ruti (2014) Regional climate model simulations indicate limited climatic
596 impacts by operational and planned European wind farms. *Nature Communications*,
597 3196, doi:10.1038/ncomms4196.

598 Warrach-Sagi, K., T. Schwitalla, V. Wulfmeyer & H. S. Bauer (2013) Evaluation of a climate
599 simulation in Europe based on the WRF-NOAH model system: precipitation in
600 Germany. *Clim. Dyn.*, 41, 755-774, doi:10.1007/s00382-013-1727-7.

601 Weisheimer, A., F. J. Doblas-Reyes, T. Jung & T. N. Palmer (2011) On the predictability of
602 the extreme summer 2003 over Europe. *Geophys. Res. Lett.*, 38, L05704, doi:
603 10.1029/2010GL046455.

604 Wild, M., B. Trussel, A. Ohmura, C. N. Long, G. König-Langlo, E. G. Dutton & A. Tsvetkov
605 (2009) Global dimming and brightening: An update beyond 2000. *J. Geophys. Res.*,
606 114, D00D13, doi: 10.1029/2008JD011382.

607 Wohlfahrt, G., S. Pilloni, L. Hörtnagl & A. Hamerle (2010) Estimating carbon dioxide fluxes
608 from temperature mountain grasslands using broad-band vegetation indices.

609 *Biogeosciences*, 7, 683-694.

610 Zhang, C., Y. Wang & K. Hamilton (2011) Improved representation of boundary layer clouds

611 over the southeast pacific in ARW-WRF using a modified Tiedtke cumulus

612 parameterization scheme. *Mon. Wea. Rev.*, 139, 3489-3513.

613 **Table and figure captions**

614

615 Table 1. Physics schemes used in this study (with references). All possible permutations are
616 made, yielding a total of 216 simulations. The numbers in the table refer to the number the
617 schemes have in the Weather Research and Forecasting (WRF) model.

618

619 Table 2. The five best performing combinations of physics in ranked from the first to the fifth
620 best.

621

622 Table 3. Cross-comparison between France 2003 and Russia 2010. The (5, 10, 15, 20 and 25)
623 best simulations, when only using one heat wave to select the best configurations and vice
624 versa, are taken and compared with their ranking for the other heat wave. If there would be no
625 correlation between the two years, the average ranking would lay approximately at half of the
626 total number of simulations for both years that lay within a first selection of 1K (column 8). In
627 bold the rankings that are lower than this number. Because observations of radiation are
628 lacking over Russia, we tested France with and without including radiation in the ranking.

629

630 Figure 1. Time series of daily land heat fluxes in 2003 from May to the end of August on
631 three different FLUXNET sites, with latent heat flux (LH) on the first row, sensible heat flux
632 (SH) on the second row, and evaporative fraction (EF – latent heat flux divided by the sum of
633 latent and sensible heat flux) on the last row. The three columns represent three sites, with
634 Neustift/Stubai (Austria – ATneu 47N, 11E) in the first column, Tharandt (Germany –
635 DETha, 51N, 4E) in the second, and Soroe-LilleBogeskov (Denmark – DKsor, 66N, 11E) in
636 the third column. Vegetation types on the three sites are respectively grassland (GRA),
637 evergreen needleleaf forest (ENF), and deciduous broadleaf forest (DBF). In grey all 216

638 simulations with the NOAH scheme. Observational data is shown in black (FLUXNET). The
639 solid light blue line is one configuration with NOAH, while the blue dots represent the same
640 configuration but with RUC instead of NOAH.

641

642 Figure 2. Domains used in this study: France, Iberian Peninsula, Russia and Scandinavia.

643

644 Figure 3. Time series of daily mean temperature over France in 2003 (a) and 2007 (b) and
645 Russia in 2010 (c). Every simulation is shown in gray and observations of E-OBS in black.
646 The blue and red lines are the coldest and the warmest simulations over France during the
647 heat wave. These lines have the same set of physics in all the figures (3, 4, 5). Figure d shows
648 the simulated temperature min-max range during the heatwave of 2003 (1-15 August). The
649 range is calculated as the difference between the warmest and the coldest simulation during
650 the heat wave period between the 216 members of the ensemble.

651

652 Figure 4. Monthly precipitation over France in 2003 (a) and 2007 (b) and Russia 2010 (c).
653 The boxplots show the extremes, 25th, 50th, and 75th percentiles. The blue and red dots are the
654 coldest and the warmest simulations over France during the heat wave (as in figure 3).

655

656 Figure 5. Scatter plot of soil moisture content at July 31, and temperature in August. Every
657 point is one simulation. Different colors and symbols represent different physics for
658 convection (CU) (a), microphysics (MP) (b), radiation (RA) (c) and planetary boundary layer-
659 surface (PBL-SF) (d).

660

661 Figure 6. Monthly radiation over France in 2003 (a) and 2007 (b); no radiation data being
662 available in Russia for 2010. The boxplots show the extremes, 25th, 50th, and 75th percentiles.

663 The blue and red dots are the coldest and the warmest simulations over France during the heat
664 wave (as in figure 3).

665

666 Figure 7. Daily time series of temperature (a) and latent heat flux (c); monthly time series of
667 precipitation (b) and incoming shortwave radiation (d). Observations are shown in black, and
668 the five best performing runs in colors. Gray lines indicate other simulations. All figures are a
669 spatial average over France during summer 2003.

670

671 Figure 8. Sensitivity test of the initialization of soil moisture. Difference between the ‘control’
672 simulation and the perturbed ones (minus (red) and plus (blue) 20% initial soil moisture) of
673 the five highest ranked configurations. The darkest lines are the best simulations (1), and
674 descending colour shade agrees with descending ranking (1-5).

Microphysics (MP)	PBL+Surface (PBL-SF)	Radiation (RA)	Convection (CU)	Soil
6) WRF-SM6 (Hong et al. 2006a)	1-1) Yonsei Uni- MM5 (Hong et al. 2006b; Beljaars, 1994)	3) CAM (Collins et al. 2004)	1) Kain-Fritsch (Kain 2004)	2) NOAH (Tewari et al. 2004)
8) New Thompson (Thompson et al. 2008)	2-2) MYJ-ETA (Janjic et al. 1994; Janjic, 2002)	4) RRTMG (Iacono et al. 2008)	3) Grell-Devenyi (Grell & Devenyi, 2012)	
10) Morrison DM (Morrison et al. 2009)	4-4) QNSE-QNSE (Sukoriansky et al. 2005)	5) Goddard (Chou & Suarez, 1999)	6) Tiedtke (Tiedtke 1989; Zhang et al. 2011)	
	5-2) MYNN-ETA (Nakanishi & Niino, 2006, 2009; Janjic, 2002)		14) New SAS (Han & Pan, 2011)	
	5-5) MYNN- MYNN (Nakanishi & Niino, 2006, 2009)			

	7-1) ACM2-MM5 (Pleim 2007; Beljaars, 1994)			
--	--	--	--	--

Microphysics	PBL-Surface	Radiation	Convection	Soil	Rank
Morrison DM	Yonsei Uni- MM5	RRTMG	Tiedtke	NOAH	1
WRF-SM6	MYNN- MYNN	RRTMG	Grell-Devenyi	NOAH	2
WRF-SM6	ACM2-MM5	Goddard	Tiedtke	NOAH	3
New Thompson	MYNN- MYNN	RRTMG	New SAS	NOAH	4
New Thompson	ACM2-MM5	RRTMG	Tiedtke	NOAH	5

680 **Table 3**

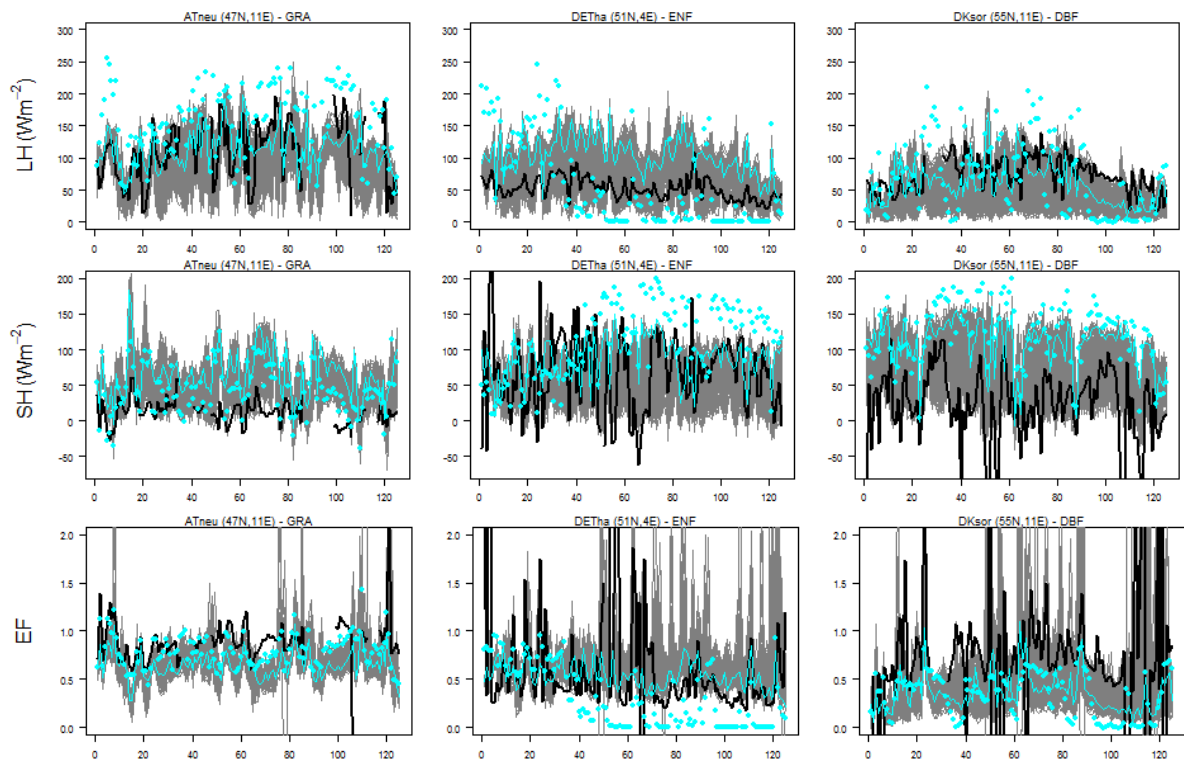
681

		Average ranking of 5, 10, 15, 20 and 25 best simulations					
		5	10	15	20	25	Number of simulations within 1°C
With radiation	Average rank Fr-Ru	22.6	21.8	25.3	23.1	27.5	104
With radiation	Average rank Ru-Fr	15.75	15.2	14.7	13	39.3	58
Without radiation	Average rank Fr-Ru	53	37	28.4	27.6	25.5	104
Without radiation	Average rank Ru-Fr	20.25	16.8	18.1	17	19.9	58

682

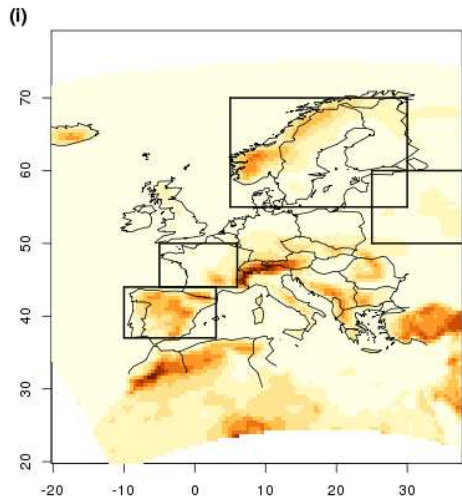
683

684 **Figure 1**

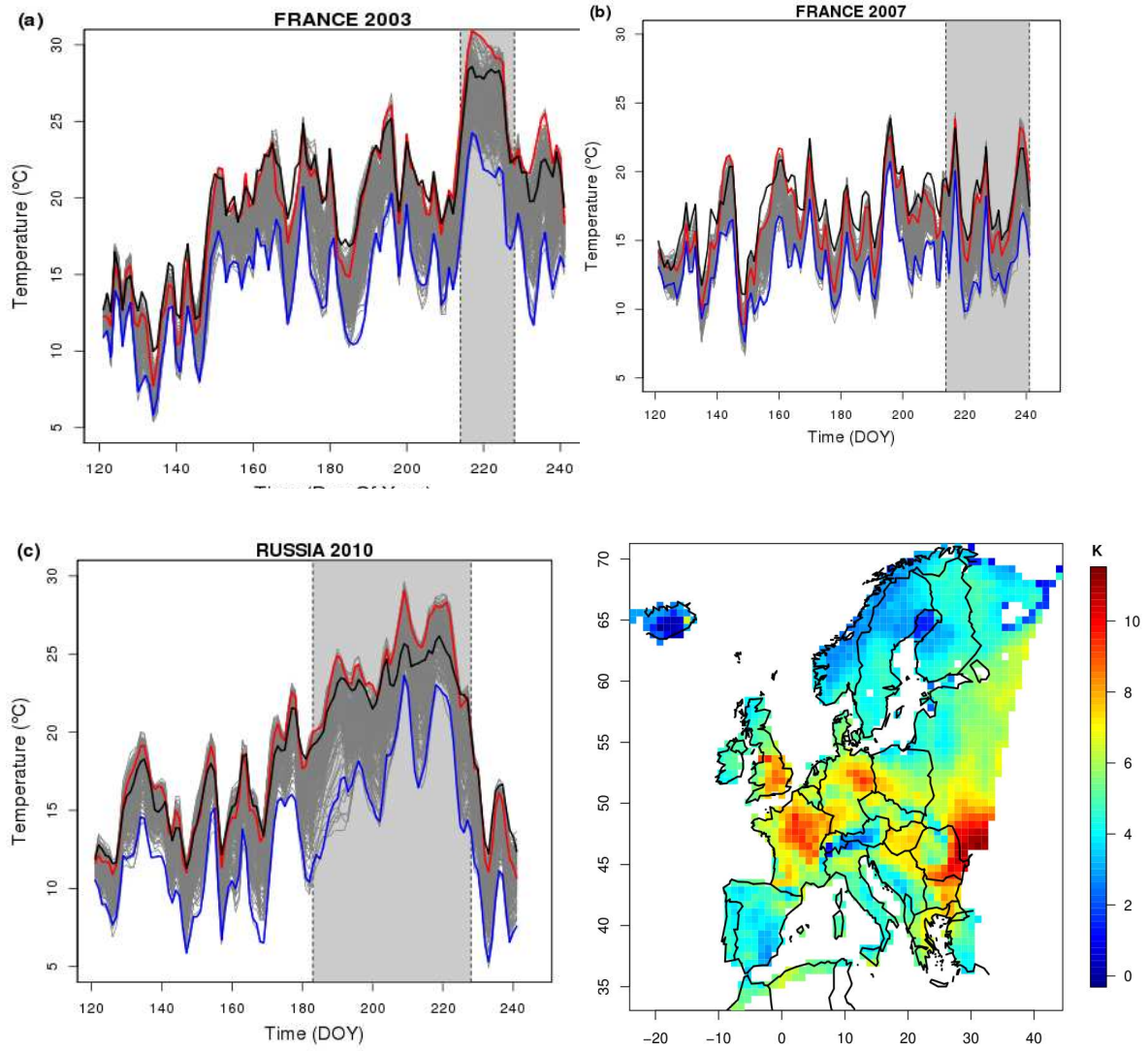


685

686
687



690 **Figure 3**



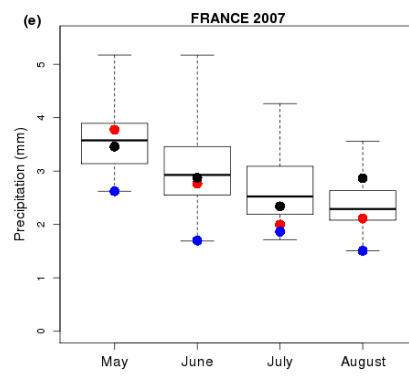
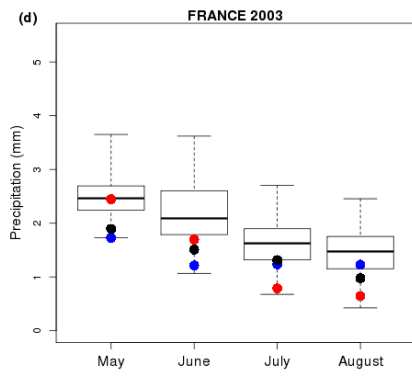
691

692

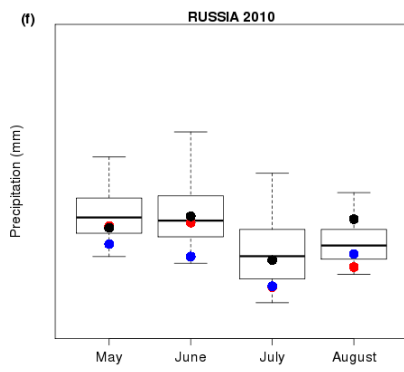
693

694 **Figure 4a-c**

695

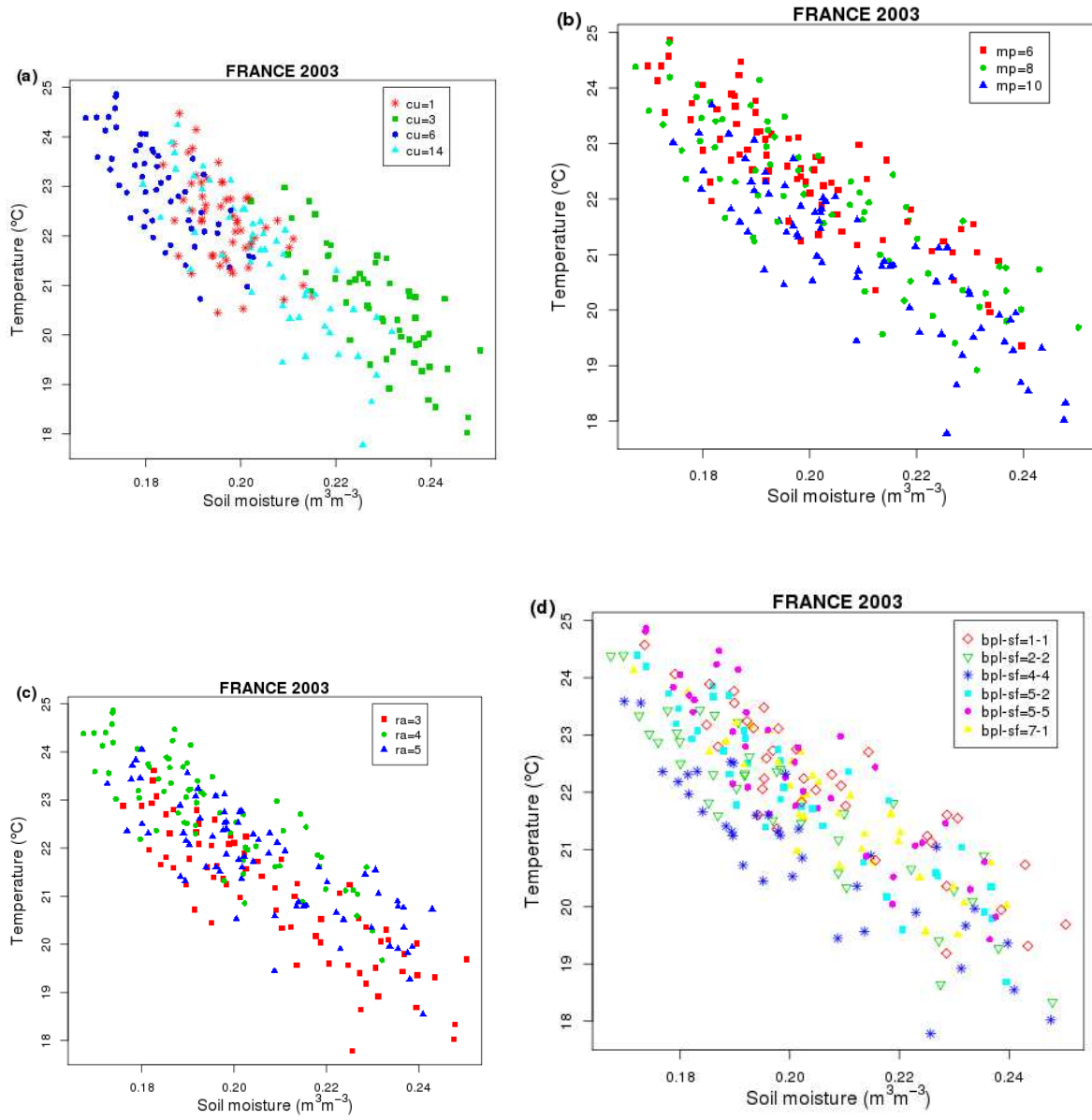


696



697

698



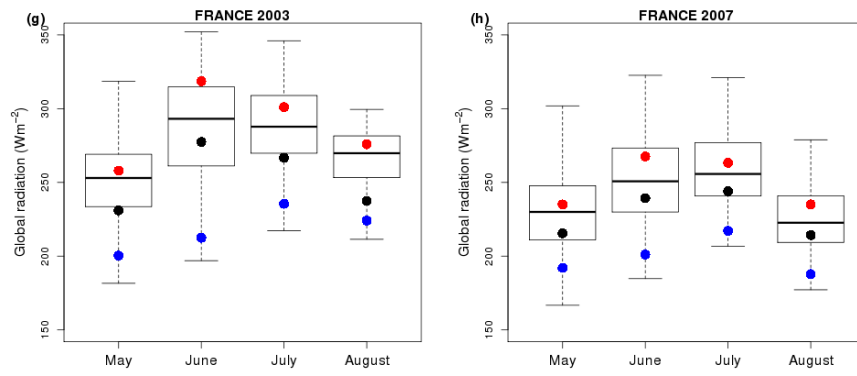
700

701

702

703

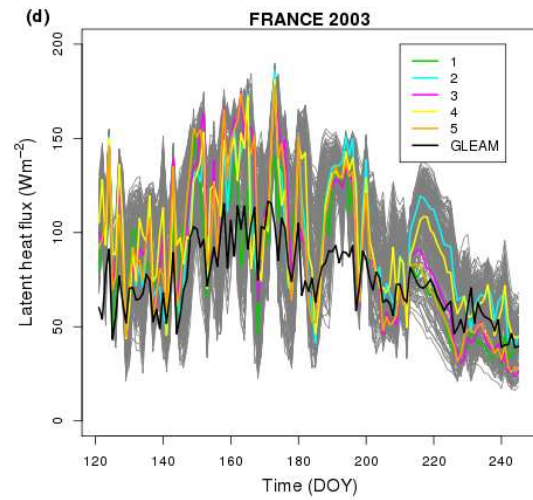
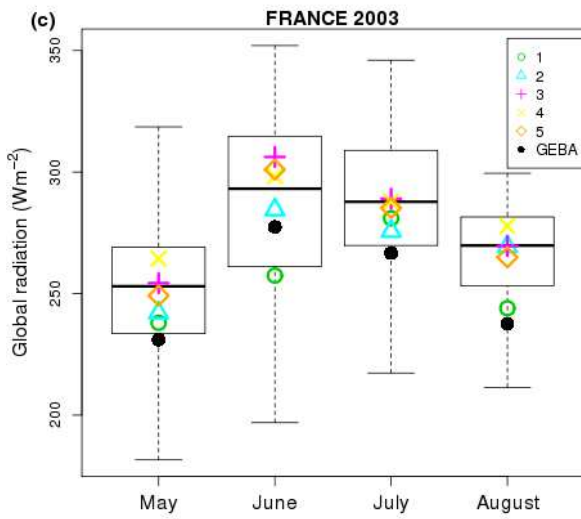
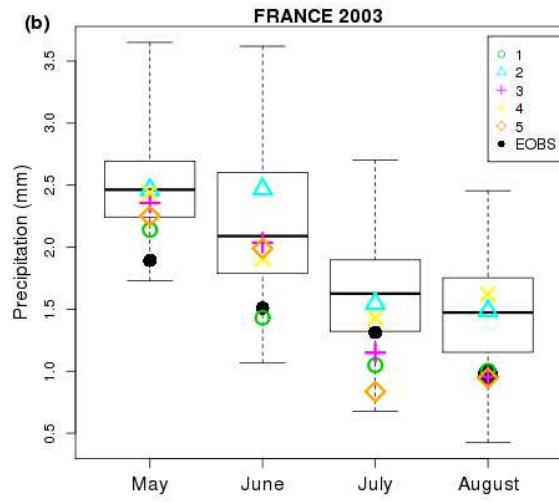
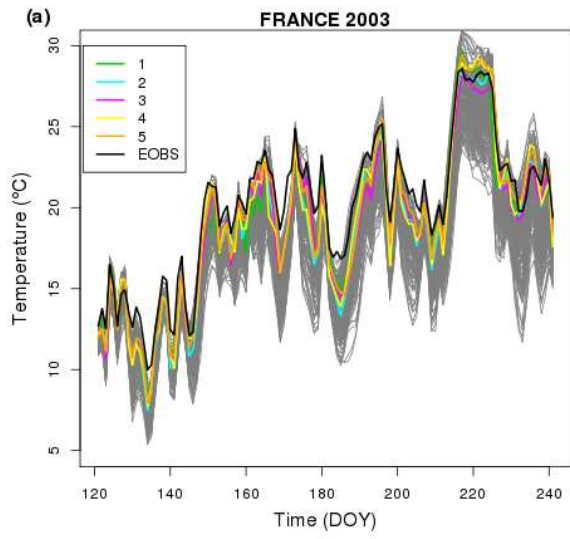
704 **Figure 6a-b**



705

706

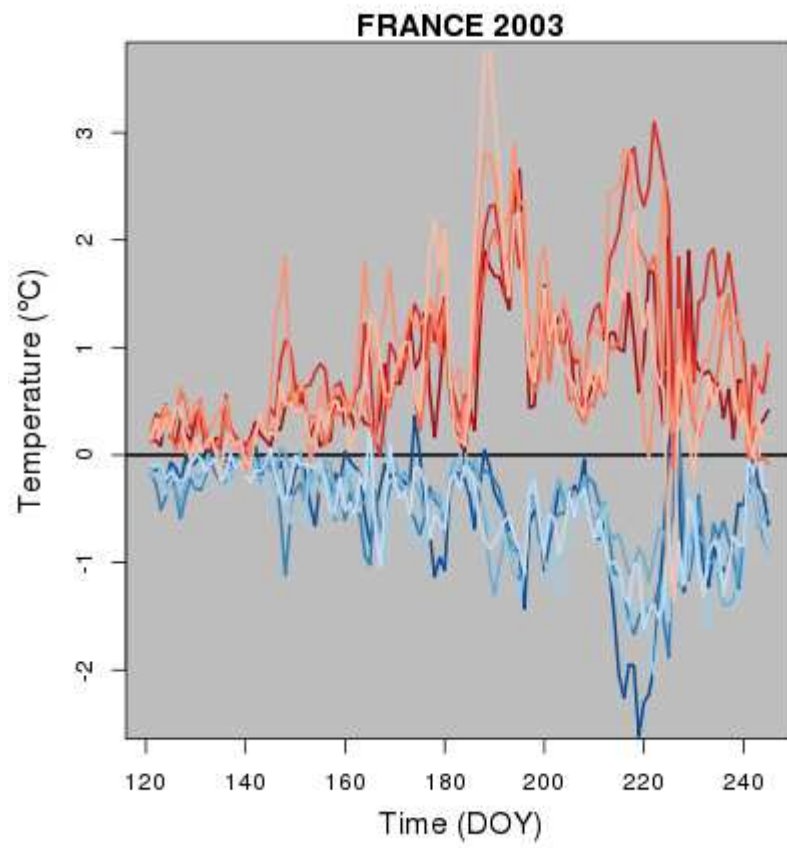
707



709

710

711 **Figure 8**



712

713